

1 **Southern Ocean heat storage, reemergence, and winter sea-ice decline**
2 **induced by summertime winds**

3 Edward W. Doddridge*

4 *Earth, Atmospheric and Planetary Sciences, Massachusetts Institute of Technology, 77*
5 *Massachusetts Avenue, Cambridge, 02139, USA, and Australian Antarctic Program Partnership,*
6 *Institute for Marine and Antarctic Studies, University of Tasmania, 20 Castray Esplanade,*
7 *Hobart, 7001, Australia*

8 John Marshall

9 *Earth, Atmospheric and Planetary Sciences, Massachusetts Institute of Technology, 77*
10 *Massachusetts Avenue, Cambridge, 02139, USA*

11 Hajoon Song

12 *Department of Atmospheric Sciences, Yonsei University, 50 Yonsei-ro, Seodaemun-gu, Seoul,*
13 *03722, South Korea*

14 Jean-Michel Campin

15 *Earth, Atmospheric and Planetary Sciences, Massachusetts Institute of Technology, 77*
16 *Massachusetts Avenue, Cambridge, 02139, USA*

17 Maxwell Kelley

18 *NASA Goddard Institute for Space Studies, 2880 Broadway, New York, NY 10025 USA*

¹⁹ **Corresponding author*: Edward W. Doddridge, edward.doddridge@utas.edu.au

ABSTRACT

20 The observational record shows a substantial 40-year upward trend in summertime westerly winds
21 over the Southern Ocean, as characterised by the Southern Annular Mode (SAM) index. Enhanced
22 summertime westerly winds have been linked to cold summertime sea surface temperature (SST)
23 anomalies. Previous studies have suggested that an Ekman transport mechanism is responsible for
24 this seasonal cooling. Here, another equally important process is presented in which cooling, driven
25 by summertime wind-induced enhanced vertical mixing, moves heat downwards, cooling the sea
26 surface and warming subsurface waters. The anomalously cold SSTs draw heat from the atmosphere
27 into the ocean, leading to enhanced depth-integrated ocean heat content. The subsurface heat is
28 returned to the surface mixed layer during the autumn and winter as the mixed layer deepens,
29 leading to anomalously warm SSTs and potentially reducing sea ice cover. Observational analyses
30 and numerical experiments support this mechanism, showing that enhanced vertical mixing drives
31 subsurface warming and cools the surface mixed layer. Anomalous advection also contributes to
32 the surface cooling, but the relative importance of advective and mixing contributions is model
33 dependent. Modeling results suggest that sea ice volume is more sensitive to summertime winds
34 than sea ice extent, implying that enhanced summertime westerly winds may lead to thinner sea ice
35 in the following winter, if not lesser ice extent. Thus, strong summertime winds could precondition
36 the sea ice cover for a rapid retreat in the following melt season.

37 **1. Introduction**

38 Each year approximately 15 million square kilometers of sea ice forms and subsequently melts in
39 the seasonal ice zone of the Southern Ocean (Fetterer et al. 2017). The buoyancy fluxes associated
40 with this seasonal ice cycle play an important role in the meridional overturning circulation in the
41 Southern Ocean (Abernathy et al. 2016; Haumann et al. 2016). This connects the surface with the
42 abyss and is a conduit for exchange between reservoirs of heat, carbon, and nutrients (Sarmiento
43 et al. 2004) in the ocean and the atmosphere. To predict how the climate system will respond
44 to anthropogenic influences we need to be able to capture changes to the overturning circulation
45 which itself demands understanding of the processes that affect the seasonal growth and decay of
46 sea ice in the Southern Ocean.

47 Sea ice extent around Antarctica has exhibited a gradual increase from the beginning of the
48 satellite record in the late 1970s. This is likely to be causally linked to the strengthening of the
49 surface westerlies blowing around Antarctica during the same period. As described by, for example,
50 Ferreira et al. (2015), Purich et al. (2016), Doddridge and Marshall (2017) and Kostov et al. (2017),
51 the enhanced summertime westerly winds associated with the positive phase of the SAM lead to a
52 rapid cooling of the SST on a timescale of weeks to months. Two advective mechanisms have been
53 proposed to explain the cold summertime SST anomalies associated with a positive summertime
54 SAM: anomalous northwards Ekman transport moving fluid across the meridional temperature
55 gradient (Ferreira et al. 2015; Kostov et al. 2017), and anomalous vertical advection due to Ekman
56 pumping drawing cold subsurface water upwards into the mixed layer (Purich et al. 2016). In
57 contrast to these two advective mechanisms, Doddridge et al. (2019) suggested that enhanced near
58 surface vertical mixing may contribute to the cold surface anomalies by mixing surface heat to
59 depth, creating anomalously warm temperatures just below the zonal-mean mixed layer depth. In an

60 observational study, Doddridge and Marshall (2017) showed that cold summertime SST anomalies
61 associated with a positive summertime SAM lead to enhanced growth of sea ice in the autumn. The
62 data suggested that there may also be a small reduction in sea ice extent at the wintertime maximum.
63 However, substantial interannual variability and a relatively short observational record, prevented
64 the identification of a statistically significant signal in wintertime sea ice extent. Motivated by the
65 observational analysis of Doddridge and Marshall (2017) and the enhanced mixing reported by
66 Doddridge et al. (2019), we return to these themes in this paper.

67 As summarised in Figure 1, we propose a vertical-mixing mechanism in which summertime
68 wind anomalies sequester heat below the mixed layer, cooling the surface. This draws heat in to
69 the surface ocean from the atmosphere adding to the heat stored in the column. As the mixed layer
70 deepens in the autumn and winter, this heat sequestered in the summer reemerges, warming SSTs,
71 reducing sea-ice volume and potentially sea ice cover. We explore these ideas in the observations,
72 in an idealised channel model of the seasonal ice zone, and in a comprehensive coupled climate
73 model.

74 Our paper is set out as follows. In section 2 we describe the climatology of the Southern Ocean
75 and present our new mechanism. In section 3 we analyse observational datasets and find some
76 evidence to support our new mechanism. In an effort to reduce the uncertainties in our analysis
77 we turn to numerical models in sections 4 and 5, where we find strong evidence that enhanced
78 summertime winds lead to increased vertical mixing and the subsurface sequestration of heat. We
79 then summarise our findings and present our conclusions in section 6.

80 **2. Vertical mixing and the seasonal sequestration of heat**

81 The time-mean circulation of the extratropical atmosphere in the southern hemisphere is dom-
82 inated by a strong westerly jet over the Southern Ocean (figure 2). Surface winds are the major

83 source of energy for the oceanic circulation (Wunsch 1998) and contribute substantially to mixing
84 (Munk and Wunsch 1998), including to the formation of the surface mixed layer (Pollard et al.
85 1972; Wunsch and Ferrari 2004). The variability of the atmospheric circulation in the southern
86 hemisphere is dominated by the Southern Annular Mode (SAM) (Gong and Wang 1999; Thompson
87 and Wallace 2000). The positive phase of the SAM is associated with a strengthening and poleward
88 shift of the midlatitude westerly winds (Thompson and Wallace 2000). Both the summertime and
89 annual mean SAM have become increasingly positive since the middle of the 20th Century (Jones
90 et al. 2016; Marshall 2003) due to anthropogenic emissions of ozone depleting substances and
91 greenhouse gases (see e.g. Polvani et al. 2011; Swart and Fyfe 2012; Thompson et al. 2011).

92 The positive trend in the SAM over the latter part of the 20th century (Jones et al. 2016) has
93 contributed to an increase in wind stress variance and more near inertial energy in the Southern
94 Ocean (Rath et al. 2014). This near inertial wind stress variability has a large impact on the
95 circulation of the Southern Ocean (Munday and Zhai 2017) and generates near-inertial waves that
96 increase mixing in the upper ocean (Furuichi et al. 2008; Rath et al. 2014; Song et al. 2019; Zhai
97 et al. 2009). We should therefore expect that the zonal wind changes associated with the SAM will
98 affect the depth of the surface mixed layer. This intuition is supported by the results of Panassa
99 et al. (2018), who found that the stronger zonal winds associated with the positive phase of the
100 SAM leads to deeper summertime mixed layers in the Southern Ocean.

101 The Southern Ocean mixed layer serves as a gateway between the subsurface ocean and the
102 atmosphere (Klocker 2018; Marshall 1997) and the seasonal cycle in the depth of the mixed layer
103 regulates a range of physical and biogeochemical processes (Doney et al. 2004; Williams et al.
104 2017). The Southern Ocean mixed layer is shallowest during the summer months (Holte et al.
105 2017), when the cold remnants of the previous winter's mixed layer are capped by a warmer surface
106 layer. This thermal structure is crucial for our mechanism, since it supplies a large reservoir of

107 cold water that can be readily accessed by the surface mixed layer. Any process that acts to deepen
108 the summertime mixed layer will cool the surface waters and warm the fluid that was previously
109 below the base of the summertime mixed layer.

110 Doddridge et al. (2019) found that stronger westerly winds associated with the positive phase
111 of the SAM created a region of warming just below the zonal-mean mixed layer depth in both
112 observations and models. A heat budget analysis of their simulations showed that this warming
113 was due to enhanced vertical mixing. Since mixing can only redistribute heat, this enhanced
114 vertical mixing must also contribute to the observed surface cooling that has previously been
115 ascribed to purely advective mechanisms (Ferreira et al. 2015; Purich et al. 2016). The presence
116 of anomalously cold water at the sea surface will affect air-sea heat fluxes; if the surface ocean
117 is anomalously cold, then the air-sea heat flux feedback will act to reduce the SST anomaly by
118 transferring heat from the atmosphere into the ocean (Hausmann et al. 2017). We therefore expect
119 an anomalously cold surface ocean to absorb additional heat from the atmosphere, leading to a
120 positive depth integrated ocean heat content anomaly. As the mixed layer deepens during autumn
121 and winter, the subsurface heat will be returned to the surface where it may affect the growth of sea
122 ice and reduce sea ice extent or volume. Our proposed mechanism is summarized schematically in
123 figure 1. In the following sections we use observational datasets and numerical experiments to test
124 our proposed mechanism and explore the relationship between the SAM, zonal-mean temperature,
125 and sea ice.

126 **3. Analysis of the seasonal cycle of Southern Ocean upper-ocean heat storage from Argo data**

127 We begin by regressing an observational time series of the summertime (December-January-
128 February, henceforth DJF) SAM (Marshall 2003) against zonal-mean temperature from a gridded
129 Argo product, an extension of the dataset described by Roemmich and Gilson (2009). By comparing

130 the magnitude of the heat content anomalies in the mixed layer and below we may be able to infer
131 the mechanism responsible for cooling the mixed layer. If the two heat content anomalies are
132 of equivalent magnitudes, then we require a mechanism that both cools the surface and warms
133 the subsurface at equivalent rates, which is consistent with enhanced vertical mixing creating the
134 temperature anomalies. However, if the cooling in the mixed layer is much larger than the warming
135 below, then it is likely that advection is the dominant mechanism driving mixed layer temperature
136 changes.

137 The Argo dataset has monthly temporal resolution, but excludes the seasonal ice zone. Figure 3a
138 shows the calculated zonal-mean temperature anomaly in February per unit DJF SAM, and clearly
139 exhibits a vertical dipole centered around the February zonal-mean mixed layer depth from Holte
140 et al. (2017). A region of surface warming is also visible to the north of the vertical dipole. This
141 warming occurs where the westerly winds weaken during a positive SAM. The warming could be
142 due either to anomalous southward Ekman transport, or by reduced vertical mixing. Our focus
143 here is on the vertical cooling/warming dipole to the south, and we will not be analyzing the
144 patch of warming to the north. By taking a volumetric integral of these temperature anomalies
145 we can calculate the associated ocean heat content anomaly per unit DJF SAM for both the mixed
146 layer and a 100 m thick region below the mixed layer (colored boxes in figure 3a). As the mixed
147 layer deepens over the seasonal cycle, the volume over which we integrate to calculate the mixed
148 layer heat content anomaly changes. Since the subsurface region is defined as a 100 m thick layer
149 beginning at the base of the zonal-mean mixed layer, this region moves but its volume remains
150 constant (to within the accuracy of the thin-shell approximation (Vallis 2006)). During the autumn
151 and winter months much of the fluid that is initially in our "below mixed layer" region is entrained
152 into the mixed layer.

153 The ocean heat content anomaly in the mixed layer has approximately the same magnitude as the
154 heat content anomaly in the fluid below the mixed layer. The fact that these two ocean heat content
155 anomalies have roughly equivalent magnitudes, but opposite signs is consistent with our hypothesis
156 that enhanced vertical mixing redistributes heat downwards from the surface. The sum of the two
157 heat content anomalies is approximately zero, but the large uncertainty means that we are unable to
158 rule out an advective contribution to the observed cooling in the mixed layer. By considering the
159 evolution of the heat content anomalies we can also assess the evidence for anomalous surface heat
160 fluxes. With an atmospheric damping rate of $5-10 \text{ W m}^{-2} \text{ K}^{-1}$ in the Southern Ocean (Hausmann
161 et al. 2016), the expected integrated anomalous heat flux into the ocean is within the uncertainty
162 range of our calculated anomalous heat contents (figure 3b). This suggests that the expected heat
163 flux signal is too small to be reliably extracted using this methodology and the available data.

164 The analysis presented by Doddridge and Marshall (2017) (their figure 3c) showed a transient
165 increase in sea ice extent due to the summertime SAM. Following Doddridge and Marshall (2017),
166 we use the Sea Ice Index, version 3 produced by Fetterer et al. (2017) to assess sea ice extent and
167 the National Oceanic and Atmospheric Administration (NOAA) Optimal Interpolation, version
168 2 dataset for sea ice concentration and SST (Reynolds et al. 2002). Repeating the analysis from
169 Doddridge and Marshall (2017) with the additional data now available does not qualitatively alter the
170 conclusions; the sea ice extent anomaly is largest in April, and then decreases, becoming negative
171 by the end of the year (see figure 3c). However, due to the substantial interannual variability we are
172 unable to find evidence supporting the influence of our mechanism on wintertime sea ice extent in
173 the observational record.

174 While our observational analysis is consistent with enhanced vertical mixing driving these zonal-
175 mean temperature anomalies, it is not conclusive. In order to further explore the driving mechanism

176 behind the observed vertical dipole in anomalous zonal-mean temperature, we turn to numerical
177 models.

178 **4. Analysis of an idealized channel model of the ACC and its seasonal ice zone**

179 We now turn to an idealized channel model of the ACC and its seasonal ice zone to further explore
180 the response of the Southern Ocean to summertime perturbations in the westerly winds. Using
181 a model allows us to diagnose heat budgets and isolate mechanisms driving change. A snapshot
182 of the model state in October (austral spring) is shown in figure 4, which clearly highlights the
183 eddying nature of the flow field.

184 The model is a reentrant channel, 3,200 km wide, 1,200 km long, and 4 km deep. The bathymetry
185 for this model consists of a 300 m deep continental shelf at the southern boundary, which then
186 slopes down to a flat bottom at 4,000 m depth for the rest of the domain. The horizontal resolution
187 is 4 km and so resolves the oceanic mesoscale eddy field, which has been shown to play a leading-
188 order role in the dynamics of the Southern Ocean (see e.g. Marshall and Radko 2003; Marshall
189 and Speer 2012; Munday et al. 2013). Further details of our numerical setup can be found in
190 Doddridge et al. (2019). While our model includes an interactive sea ice (Losch et al. 2010) it lacks
191 an interactive atmosphere, which precludes the study of coupled ocean-atmosphere phenomena.
192 We use a repeating seasonal cycle of surface forcings that are derived from the Co-ordinated
193 Ocean-Ice Reference Experiments (CORE) Corrected Normal Year Forcing Version 2.0 (CNYF)
194 (Large and Yeager 2004).

195 The MITgcm (Marshall et al. 1997a,b) is used to solve the equations of motion, and the scientific
196 Python stack to analyze the output (Hoyer and Hamman 2017; Hunter 2007; Kluyver et al. 2016;
197 Perez and Granger 2007; Van Der Walt et al. 2011).

198 We begin by analyzing ensembles of idealized channel model simulations. After spinning up
199 to a statistical equilibrium, we create two ensembles, one to establish the control and the other
200 the perturbation about the control. To create a member of the perturbation ensemble we restart
201 the model from a checkpoint with altered summertime zonal winds, surface air temperature, and
202 surface humidity that mimic the positive phase of the SAM (see Doddridge et al. (2019) for details
203 of the perturbations). In our idealized model we represent only the strengthening of the zonal
204 winds, neglecting the potential impact of a meridional shift (c.f. Waugh et al. 2019). This means
205 that we do not expect the channel model to reproduce the patch of surface warming seen in the
206 observations (figure 3).

207 We use six snapshots from the control simulation as initial conditions for the perturbation
208 ensemble members, with each set of initial conditions separated from the previous state by one
209 year of model time. The control ensemble is created by using the same checkpoints, but continuing
210 the simulation without altering the atmospheric fields. Averaging multiple ensemble members
211 helps to reduce the impact of the vigorous mesoscale eddy field on our results.

212 One month after applying the wind perturbation the mixed layer is deeper and colder in the
213 perturbation ensemble than the control ensemble (figures 5 and 6a) (c.f. Sallée et al. 2010). The
214 mixed layer depth in our idealized channel model is calculated using the density-based
215 criterion of Kara et al. (2000) with $\Delta T = 0.8^{\circ}\text{C}$. There is also a region of anomalous warmth
216 just below the zonal-mean mixed layer depth (figure 6a). A heat budget shows that the negative
217 temperature anomaly in the mixed layer and the positive temperature anomaly in the region below
218 are both predominantly caused by enhanced vertical diffusion (figure 6b). Both horizontal and
219 vertical advection contribute to the cooling in the mixed layer, suggesting that the advective
220 mechanisms proposed by Ferreira et al. (2015) and Purich et al. (2016) are also active in this
221 model. However, the advective contributions are approximately an order of magnitude smaller

222 than the cooling due to vertical diffusion (figure 6b). The dominance of vertical mixing is further
223 corroborated by the integrated ocean heat content anomalies (figure 7). During the first summer
224 the anomalous cooling in the mixed layer is slightly larger than the magnitude of the anomalous
225 warming below the zonal-mean mixed layer depth, consistent with a small contribution from
226 advection.

227 As predicted, there is an anomalous flux of heat into the ocean through the surface (not shown),
228 which causes the total upper ocean heat content anomaly to increase (green line, figure 7). During
229 autumn, the mixed layer deepens and returns the anomalously warm water below the zonal-mean
230 mixed layer depth to the surface. In conjunction with the anomalous surface heat fluxes, this causes
231 the mixed layer to become anomalously warm during the winter months (blue line, figure 7) and
232 reduces sea ice volume (red line, figure 7). Our idealized channel model fails to reproduce the
233 transient increase in sea ice extent found by Doddridge and Marshall (2017) in the observations.
234 This is likely due to the sea ice edge being too far south to be substantially affected by the
235 anomalously cold SST; by the time the sea ice edge extends far enough north to interact with the
236 SST anomaly, the mixed layer has become anomalously warm.

237 **5. Analysis of the GISS coupled climate model**

238 While the zonal-mean temperature anomalies in our idealized channel model have much in
239 common with those found in the observations, both in pattern and amplitude, the idealized nature
240 of that model raises questions about how widely applicable the results are. We therefore seek to test
241 our proposed mechanism in another model, one that is global and fully coupled, with interactive
242 atmosphere, ice, and ocean components. We use the most recent National Aeronautics and Space
243 Administration (NASA) Goddard Institute for Space Studies (GISS) global coupled model, Model
244 E2.1, in the configuration described by Doddridge et al. (2019). A major caveat is that due to

245 the added complexity, this model is run at a much coarser resolution and mesoscale eddies are
246 parameterized rather than explicitly resolved. The model includes a Gent-McWilliams style eddy
247 parameterization (Gent and McWilliams 1990; Gent et al. 1995) with a flow-dependent variable
248 eddy diffusivity. Further details of the model and our numerical setup can be found in Doddridge
249 et al. (2019), Kelley et al. (2020), and Miller et al. (2020).

250 The climatology of the control configuration of this model closely resembles the observed
251 climatology of the Southern Ocean; figure 8 shows the surface climatology in the Southern Ocean
252 for the summertime sea ice minimum in February (a) and the wintertime sea ice maximum in
253 September (b). From an equilibrated preindustrial control simulation we spawn an ensemble of
254 perturbation experiments by imposing a stratospheric ozone hole mimicking the conditions in
255 the 1990s (see Doddridge et al. (2019) for details of the ozone hole perturbation). The imposed
256 ozone depletion causes the summertime SAM to become anomalously positive and enhances the
257 summertime westerly winds (Polvani et al. 2011). Once again we construct a control ensemble
258 by combining the equivalent unperturbed simulations and define the anomaly as the difference
259 between the two ensemble means. We will now use these ensembles to assess the influence of our
260 mechanism in a global coupled model.

261 The zonal-mean temperature perturbation clearly shows a vertical dipole (figure 9a). A heat
262 budget for the mixed layer reveals that the cooling is largely driven by advection, with diffusion
263 making a small contribution (figure 9b). The warming is located below the zonal-mean mixed layer
264 depth from the control ensemble, and our heat budget analysis reveals that diffusion is the largest
265 contributor to this warming (figure 9c). Calculating the ocean heat content anomaly in the mixed
266 layer and the region below the mixed layer shows that the cooling in the mixed layer is larger than
267 the warming below, consistent with advectively driven cooling. Because the model fields required

268 to decompose the advective contribution into horizontal and vertical components are not available,
269 we cannot assess which of the two advective hypotheses this model supports.

270 To allow for easier comparison with the observational analysis in section 3 and Doddridge and
271 Marshall (2017), we will switch from analyzing differences between the control and perturbation
272 ensembles to performing regression analyses on the control ensemble. We begin by defining an
273 analogous SAM index to the observational index from Marshall (2003). We then compute lagged
274 linear correlations between this SAM index and the zonal-mean temperature field. The predicted
275 zonal-mean temperature anomaly from a +1 SAM is shown in figure 10a. The ocean heat content
276 anomalies implied by these temperature changes are plotted in figure 10b, and show that the cooling
277 in the mixed layer is substantially larger than the warming below. The difference between the two
278 heat content anomalies is consistent with the heat budget analysis that showed advection played
279 a substantial role in cooling the mixed layer (figure 9b). To assess the sea ice response to SAM
280 perturbations we regress sea ice area and sea ice volume against the summertime SAM index.
281 We find a transient increase in both area and volume that peaks in May, following which the area
282 anomaly decreases to zero and the volume anomaly becomes negative (figure 10c). Our analysis
283 suggests that positive perturbations to the summertime SAM may reduce sea ice volume at the
284 wintertime peak in sea ice. However, the lack of statistical significance means that we are unable
285 to draw robust conclusions about the change in sea ice volume from these simulations.

286 **6. Discussion and Conclusions**

287 We have proposed a new mechanism through which summertime wind perturbations can affect
288 ocean temperature and sea ice over a seasonal timescale. According to our mechanism, strengthened
289 summertime winds lead to anomalous vertical mixing, which cools the mixed layer and warms
290 the ocean just beneath mixed layer. Due to the anomalously cold sea surface, anomalous air-sea

291 heat fluxes transfer additional heat into the surface ocean. As the mixed layer deepens during
292 the autumn months, the combined effect of the anomalous air-sea heat fluxes and entrainment of
293 anomalously warm subsurface water causes the mixed layer to become anomalously warm. This
294 would likely lead to a reduction in sea ice during the winter months, either in ice volume or ice
295 extent, or both.

296 It has previously been proposed that the surface cooling in response to strengthened westerly
297 winds is primarily due to horizontal advection (Ferreira et al. 2015) or vertical advection (Purich
298 et al. 2016). Our analysis of the observations suggests that enhanced vertical diffusion plays the
299 leading role in creating both the cold SST anomaly and the warm subsurface temperature anomaly.
300 However, due to inadequacies in data we are unable to rule out an advective contribution to the
301 observed surface cooling signal. Our idealized channel model does not support an advective
302 mechanism; the heat budget (figure 6b) clearly shows that anomalous vertical mixing is the
303 dominant cause of the cold SST anomaly, with only minor contributions from both horizontal and
304 vertical advection. This enhanced vertical mixing is also responsible for subsurface warming. In
305 our global coupled model, the subsurface warming is similarly due to enhanced vertical mixing,
306 but the mixed layer cooling is mostly due to advection, with only a small contribution from mixing.
307 The relative importance of our proposed mixing-based mechanism and the previously proposed
308 advective mechanisms (Ferreira et al. 2015; Purich et al. 2016) is therefore model dependent.
309 Given the observational uncertainty and model dependence, it is difficult to conclusively state
310 which mechanism is most important in the Southern Ocean. That said, we lend strong credence to
311 the highly resolved channel calculations presented here – because the relevant dynamics is resolved
312 – and believe that enhanced vertical diffusion is likely more important than either horizontal or
313 vertical advection.

314 Our observational analysis and our coupled global model both show that the summertime SAM
315 has little impact on the wintertime sea ice extent. However, both our idealized channel model and
316 our global coupled model show a reduction in sea ice volume in the winter following anomalously
317 strong summertime westerlies. These results suggest that sea ice volume is more sensitive to
318 summertime winds than sea ice extent. Unfortunately, we are unable to assess the relationship
319 between summertime winds and sea ice volume in the observations due to the lack of a long-term
320 time-series for sea ice volume in the Southern Ocean. If, as our modeling results suggest, stronger
321 summertime westerlies do cause a reduction in sea ice volume in the following winter, then a
322 positive DJF SAM may precondition sea ice for a rapid retreat in the following spring. Indeed there
323 was a remarkable reduction in sea ice extent observed in the austral spring of 2016 (September-
324 October-November) (Jones et al. 2016; Parkinson and Cavalieri 2012; Scambos and Stammerjohn
325 2018) which followed an unusually large and positive SAM in the summer of 2015 which may
326 have preconditioned Antarctic sea ice for the rapid springtime retreat the following year. That
327 said, the 2016 decline has been linked to numerous factors including anomalous meridional winds
328 and heat advection in the atmosphere (Schlosser et al. 2017), El Niño (Stuecker et al. 2017), and
329 to the Southern Annular Mode (SAM) (Doddridge and Marshall 2017). The breadth of proposed
330 explanations is testament to the complexity of the southern cryosphere. Exploring the contribution
331 of our mechanism to sea ice changes in specific years or locations presents an exciting avenue for
332 future work.

333 Our focus on summertime winds is motivated by the observed changes in the summertime SAM
334 (Marshall 2003), and the potential for seasonal reemergence of the sequestered heat. During
335 winter the mixed layer is substantially deeper (Holte et al. 2017), and the stratification is such that
336 additional mixing at the base of the mixed layer would warm the surface waters. It is only during
337 the summer, when a shallow thermally stratified layer forms a cap above the previous winter's

338 mixed layer, that additional mixing can cool the surface. We have therefore focused on the impacts
339 of enhanced zonal winds in the summertime.

340 Through our proposed mechanism, enhanced summertime winds drive anomalous near-surface
341 diapycnal mixing. According to Sloyan et al. (2010), summertime diapycnal mixing near the Sub-
342 antarctic Front preconditions the ocean for the rapid development of deep mixed layers and efficient
343 formation of Subantarctic Mode Water (SAMW) and Antarctic Intermediate Water (AAIW). Our
344 mechanism may therefore increase the volume of SAMW and AAIW formed (c.f. Gao et al. 2018).
345 Further analysis of the role of summertime wind anomalies on the formation of SAMW and AAIW
346 are beyond the scope of this contribution.

347 In conclusion, we have presented a novel mechanism that predicts a non-monotonic SST response
348 to summertime wind perturbations: initially the sea surface cools before warming in the winter
349 months as heat that was sequestered below the surface is returned to the surface mixed layer. Our
350 mechanism predicts that enhanced summertime westerlies will increase sea ice cover during the
351 autumn and reduce sea ice volume during winter; predictions that are supported by our modeling
352 studies and observational analysis.

353 *Data availability statement.* All observational datasets used can be obtained by following the
354 directions in the cited articles. Model configurations are described in detail in the text and cited
355 articles. Due to the expense of publicly hosting large datasets, the model output is not publicly
356 available. Interested readers should contact the corresponding author for further information or
357 access.

358 *Acknowledgments.* We thank Alex Haumann for helpful comments on an earlier draft. E. Dod-
359 dridge acknowledges support from the NSF's Antarctic program. J. Marshall acknowledges support
360 from the MIT-GISS collaborative agreement and the NSF Polar Antarctic Program. H. Song is

361 supported by Yonsei University Research Fund (2018-22-0053) and National Research Foundation
362 of Korea (NRF) grant funded by Korea government (MSIST) (NRF-2019R1C1C1003663). This
363 project received grant funding from the Australian Government as part of the Antarctic Science
364 Collaboration Initiative program. The Australian Antarctic Program Partnership is led by the
365 University of Tasmania, and includes the Australian Antarctic Division, CSIRO Oceans and Atmo-
366 sphere, Geoscience Australia, the Bureau of Meteorology, the Tasmanian State Government and
367 Australia's Integrated Marine Observing System.

368 **References**

- 369 Abernathy, R. P., I. Cerovecki, P. R. Holland, E. Newsom, M. Mazloff, and L. D. Talley, 2016:
370 Water-mass transformation by sea ice in the upper branch of the Southern Ocean overturning.
371 *Nature Geoscience*, **9 (8)**, 596–601,
- 372 Doddridge, E. W., J. Marshall, H. Song, J.-M. Campin, M. Kelley, and L. Nazarenko, 2019: Eddy
373 Compensation Dampens Southern Ocean Sea Surface Temperature Response to Westerly Wind
374 Trends. *Geophysical Research Letters*, **46 (8)**, 4365–4377,
- 375 Doddridge, E. W., and J. C. Marshall, 2017: Modulation of the Seasonal Cycle of Antarctic
376 Sea Ice Extent Related to the Southern Annular Mode. *Geophysical Research Letters*, **44 (19)**,
377 9761–9768,
- 378 Doney, S. C., and Coauthors, 2004: Evaluating global ocean carbon models: The importance of
379 realistic physics. *Global Biogeochemical Cycles*, **18 (3)**, doi:10.1029/2003GB002150.
- 380 Ferreira, D., J. C. Marshall, C. M. Bitz, S. Solomon, and A. Plumb, 2015: Antarctic ocean and
381 sea ice response to ozone depletion: A two-time-scale problem. *Journal of Climate*, **28 (3)**,
382 1206–1226, doi:10.1175/JCLI-D-14-00313.1.

383 Fetterer, F., K. Knowles, W. Meier, M. Savoie, and A. Windnagel, 2017: Sea Ice Index, Version 3
384 [south]. doi:10.7265/N5K072F8.

385 Furuichi, N., T. Hibiya, and Y. Niwa, 2008: Model-predicted distribution of wind-induced internal
386 wave energy in the world's oceans. *Journal of Geophysical Research: Oceans*, **113** (9), 1–13,
387 doi:10.1029/2008JC004768.

388 Gao, L., S. R. Rintoul, and W. Yu, 2018: Recent wind-driven change in Subantarctic Mode Water
389 and its impact on ocean heat storage. *Nature Climate Change*, **8** (1), 58–63,

390 Gent, P. R., and J. C. McWilliams, 1990: Isopycnal Mixing in Ocean Circulation Models. *Journal*
391 *of Physical Oceanography*, **20** (1), 150–155,

392 Gent, P. R., J. Willebrand, T. J. McDougall, and J. C. McWilliams, 1995: Parameterizing Eddy-
393 Induced Tracer Transports in Ocean Circulation Models. *Journal of Physical Oceanography*,
394 **25** (4), 463–474,

395 Gong, D., and S. Wang, 1999: Definition of Antarctic Oscillation index. *Geophysical Research*
396 *Letters*, **26** (4), 459–462,

397 Haumann, F. A., N. Gruber, M. Münnich, I. Frenger, and S. Kern, 2016: Sea-ice transport driving
398 Southern Ocean salinity and its recent trends. *Nature*, **537** (7618), 89–92,

399 Hausmann, U., A. Czaja, and J. C. Marshall, 2016: Estimates of Air-Sea Feedbacks on Sea Surface
400 Temperature Anomalies in the Southern Ocean. *Journal of Climate*, **29** (2), 439–454,

401 Hausmann, U., A. Czaja, and J. C. Marshall, 2017: Mechanisms controlling the SST air-sea heat
402 flux feedback and its dependence on spatial scale. *Climate Dynamics*, **48** (3-4), 1297–1307,

403 Holte, J., L. D. Talley, J. Gilson, and D. Roemmich, 2017: An Argo mixed layer climatology and
404 database. *Geophysical Research Letters*, **44** (11), 5618–5626, doi:10.1002/2017GL073426.

405 Hoyer, S., and J. J. Hamman, 2017: xarray: N-D labeled Arrays and Datasets in Python. *Journal*
406 *of Open Research Software*, **5**, 1–6, doi:10.5334/jors.148.

407 Hunter, J. D., 2007: Matplotlib: A 2D graphics environment. *Computing in Science and Engineer-*
408 *ing*, **9 (3)**, 99–104, doi:10.1109/MCSE.2007.55.

409 Jones, J. M., and Coauthors, 2016: Assessing recent trends in high-latitude Southern Hemisphere
410 surface climate. *Nature Climate Change*, **6 (10)**, 917–926,

411 Kara, A. B., P. A. Rochford, and H. E. Hurlburt, 2000: An optimal definition for ocean mixed layer
412 depth. *Journal of Geophysical Research: Oceans*, **105 (C7)**, 16 803–16 821, arXiv:1011.1669v3.

413 Kelley, M., and Coauthors, 2020: GISS-E2.1: Configurations and climatology.

414 Klocker, A., 2018: Opening the window to the Southern Ocean: The role of jet dynamics. *Science*
415 *Advances*, **4 (10)**, doi:10.1126/sciadv.aao4719.

416 Kluyver, T., and Coauthors, 2016: Jupyter Notebooks—a publishing format for reproducible
417 computational workflows. *Positioning and Power in Academic Publishing: Players, Agents and*
418 *Agendas*, 87–90, doi:10.3233/978-1-61499-649-1-87.

419 Kostov, Y., J. C. Marshall, U. Hausmann, K. C. Armour, D. Ferreira, and M. M. Holland, 2017:
420 Fast and slow responses of Southern Ocean sea surface temperature to SAM in coupled climate
421 models. *Climate Dynamics*, **48 (5-6)**, 1595–1609,

422 Large, W. G., and S. G. Yeager, 2004: Diurnal to decadal global forcing for ocean and sea-ice
423 models: The data sets and flux climatologies. *NCAR Tech. Note*, **TN-460+ST**, 105pp, doi:
424 10.5065/D6KK98Q6.

- 425 Losch, M., D. Menemenlis, J. M. Campin, P. Heimbach, and C. Hill, 2010: On the formulation
426 of sea-ice models. Part 1: Effects of different solver implementations and parameterizations.
427 *Ocean Modelling*, **33 (1-2)**, 129–144,
- 428 Marshall, D. P., 1997: Subduction of water masses in an eddying ocean. *Journal of Marine*
429 *Research*, **55 (2)**, 201–222,
- 430 Marshall, G. J., 2003: Trends in the Southern Annular Mode from Observations and Reanalyses.
431 *Journal of Climate*, **16 (24)**, 4134–4143,
- 432 Marshall, J. C., A. Adcroft, C. Hill, L. Perelman, and C. Heisey, 1997a: A finite-volume, in-
433 compressible Navier Stokes model for studies of the ocean on parallel computers. *Journal of*
434 *Geophysical Research: Oceans*, **102 (C3)**, 5753–5766,
- 435 Marshall, J. C., C. Hill, L. Perelman, and A. Adcroft, 1997b: Hydrostatic, quasi-hydrostatic, and
436 nonhydrostatic ocean modeling. *Journal of Geophysical Research: Oceans*, **102 (C3)**, 5733–
437 5752,
- 438 Marshall, J. C., and T. Radko, 2003: Residual-Mean Solutions for the Antarctic Circumpolar
439 Current and Its Associated Overturning Circulation. *Journal of Physical Oceanography*, **33 (11)**,
440 2341–2354,
- 441 Marshall, J. C., and K. Speer, 2012: Closure of the meridional overturning circulation through
442 Southern Ocean upwelling. *Nature Geoscience*, **5**, doi:10.1038/NGEO1391.
- 443 Miller, R. L., and Coauthors, 2020: CMIP6 historical simulations (1850-2014) with GISS Mod-
444 eE2.1.
- 445 Munday, D. R., H. L. Johnson, and D. P. Marshall, 2013: Eddy Saturation of Equilibrated
446 Circumpolar Currents. *Journal of Physical Oceanography*, **43 (3)**, 507–532,

447 Munday, D. R., and X. Zhai, 2017: The impact of atmospheric storminess on the sensitivity
448 of Southern Ocean circulation to wind stress changes. *Ocean Modelling*, **115**, 14–26, doi:
449 10.1016/j.ocemod.2017.05.005.

450 Munk, W., and C. Wunsch, 1998: Abyssal recipes II: energetics of tidal and wind mixing. *Deep*
451 *Sea Research Part I: Oceanographic Research Papers*, **45 (12)**, 1977–2010,

452 Panassa, E., C. Völker, D. Wolf-Gladrow, and J. Hauck, 2018: Drivers of interannual variability of
453 summer Mixed Layer Depth in the Southern Ocean between 2002-2011. *Journal of Geophysical*
454 *Research: Oceans*, **123 (8)**, 5077–5090,

455 Parkinson, C. L., and D. J. Cavalieri, 2012: Antarctic sea ice variability and trends, 1979-2010.
456 *The Cryosphere*, **6 (4)**, 871–880,

457 Perez, F., and B. E. Granger, 2007: IPython: A System for Interactive Scientific Computing.
458 *Computing in Science & Engineering*, **9 (3)**, 21–29,

459 Pollard, R. T., P. B. Rhines, and R. O. R. Y. Thompson, 1972: The deepening of the wind-Mixed
460 layer. *Geophysical Fluid Dynamics*, **4 (1)**, 381–404,

461 Polvani, L. M., D. W. Waugh, G. J. P. Correa, and S.-W. Son, 2011: Stratospheric Ozone Deple-
462 tion: The Main Driver of Twentieth-Century Atmospheric Circulation Changes in the Southern
463 Hemisphere. *Journal of Climate*, **24 (3)**, 795–812,

464 Purich, A., W. Cai, M. H. England, and T. Cowan, 2016: Evidence for link between modelled
465 trends in Antarctic sea ice and underestimated westerly wind changes. *Nature Communications*,
466 **7**, 10409, arXiv:1011.1669v3.

- 467 Rath, W., R. J. Greatbatch, and X. Zhai, 2014: On the spatial and temporal distribution of near-
468 inertial energy in the Southern Ocean. *Journal of Geophysical Research: Oceans*, **119** (1),
469 359–376,
- 470 Reynolds, R. W., N. A. Rayner, T. M. Smith, D. C. Stokes, and W. Wang, 2002: An improved
471 in situ and satellite SST analysis for climate. *Journal of Climate*, **15** (13), 1609–1625, doi:
472 10.1175/1520-0442(2002)015<1609:AIISAS>2.0.CO;2.
- 473 Roemmich, D., and J. Gilson, 2009: The 2004-2008 mean and annual cycle of temperature, salinity,
474 and steric height in the global ocean from the Argo Program. *Progress in Oceanography*, **82** (2),
475 81–100,
- 476 Sallée, J.-B., K. G. Speer, and S. R. Rintoul, 2010: Zonally asymmetric response of the Southern
477 Ocean mixed-layer depth to the Southern Annular Mode. *Nature Geoscience*, **3** (4), 273–279,
- 478 Sarmiento, J. L., N. Gruber, M. A. Brzezinski, and J. P. Dunne, 2004: High-latitude controls of
479 thermocline nutrients and low latitude biological productivity. *Nature*, **427** (6969), 56–60,
- 480 Scambos, T., and S. Stammerjohn, 2018: Antarctica [in "State of the Climate in 2017"]. *Bull.*
481 *Amer. Meteor. Soc.*, **99** (August), 175–192, doi:10.1175/2018BAMSStateoftheClimate.1.
- 482 Schlosser, E., F. A. Haumann, and M. N. Raphael, 2017: Atmospheric influences on the anomalous
483 2016 Antarctic sea ice decay. *The Cryosphere Discussions*, **2014**, 1–31,
- 484 Sloyan, B. M., L. D. Talley, T. K. Chereskin, R. Fine, and J. Holte, 2010: Antarctic intermediate
485 water and subantarctic mode water formation in the Southeast Pacific: The role of turbulent
486 mixing. *Journal of Physical Oceanography*, **40** (7), 1558–1574, doi:10.1175/2010JPO4114.1.

- 487 Song, H., J. Marshall, J. M. Campin, and D. J. McGillicuddy, 2019: Impact of Near-Inertial Waves
488 on Vertical Mixing and Air-Sea CO₂ Fluxes in the Southern Ocean. *Journal of Geophysical*
489 *Research: Oceans*, **124** (7), 4605–4617, doi:10.1029/2018JC014928.
- 490 Stuecker, M. F., C. M. Bitz, and K. C. Armour, 2017: Conditions leading to the unprecedented low
491 Antarctic sea ice extent during the 2016 austral spring season. *Geophysical Research Letters*,
492 **44** (17), 9008–9019, doi:10.1002/2017GL074691.
- 493 Swart, N. C., and J. C. Fyfe, 2012: Observed and simulated changes in the Southern Hemi-
494 sphere surface westerly wind-stress. *Geophysical Research Letters*, **39** (16), 6–11, doi:
495 10.1029/2012GL052810.
- 496 Thompson, D. W. J., S. Solomon, P. J. Kushner, M. H. England, K. M. Grise, and D. J. Karoly,
497 2011: Signatures of the Antarctic ozone hole in Southern Hemisphere surface climate change.
498 *Nature Geoscience*, **4** (11), 741–749,
- 499 Thompson, D. W. J., and J. M. Wallace, 2000: Annular Modes in the Extratropical Circulation.
500 Part I: Month-to-Month Variability. *Journal of Climate*, **13** (5), 1000–1016,
- 501 Vallis, G. K., 2006: *Atmospheric and Oceanic Fluid Dynamics*. Cambridge University Press,
502 Cambridge, UK, 745 pp.
- 503 Van Der Walt, S., S. C. Colbert, and G. Varoquaux, 2011: The NumPy array: A structure for
504 efficient numerical computation. *Computing in Science and Engineering*, **13** (2), 22–30, doi:
505 10.1109/MCSE.2011.37, 1102.1523.
- 506 Waugh, D. W., A. M. Hogg, P. Spence, M. H. England, and T. W. Haine, 2019: Response
507 of Southern Ocean ventilation to changes in midlatitude westerly winds. *Journal of Climate*,
508 **32** (17), 5345–5361, doi:10.1175/JCLI-D-19-0039.1.

- 509 Williams, N. L., and Coauthors, 2017: Calculating surface ocean pCO₂ from biogeochemical
510 Argo floats equipped with pH: An uncertainty analysis. *Global Biogeochemical Cycles*, **31** (3),
511 591–604, doi:10.1002/2016GB005541.
- 512 Wunsch, C., 1998: The Work Done by the Wind on the Oceanic General Circulation. *Journal of*
513 *Physical Oceanography*, **28** (11), 2332–2340,
- 514 Wunsch, C., and R. Ferrari, 2004: Vertical Mixing, Energy, and the General Circulation of the
515 Oceans. *Annual Review of Fluid Mechanics*, **36** (1), 281–314,
- 516 Zhai, X., R. J. Greatbatch, C. Eden, and T. Hibiya, 2009: On the Loss of Wind-Induced Near-
517 Inertial Energy to Turbulent Mixing in the Upper Ocean. *Journal of Physical Oceanography*,
518 **39** (11), 3040–3045,

519 **LIST OF FIGURES**

520 **Fig. 1.** Schematic of vertical mixing/heat sequestration mechanism. In summer, anomalous westerly
521 winds (τ' above left hand column) enhance vertical mixing at the base of the mixed layer
522 (white squiggly arrows and horizontal black line, respectively) moving heat downwards and
523 causing a vertical dipole of anomalous temperatures (colors). The anomalously cold SST
524 causes anomalous heat fluxes into the ocean during the autumn (Q' and red arrow above
525 central column), which reduces the cold SST anomaly. As autumn progresses, the mixed
526 layer continues to deepen, entraining the anomalously warm fluid sequestered below the
527 zonal-mean mixed layer depth. Due to the anomalous surface heat fluxes, which increases
528 the total heat content of the upper ocean, the mixed layer is now anomalously warm. This
529 can be expected to lead to a reduction in wintertime sea ice. 28

530 **Fig. 2.** Climatology of the Southern Ocean. Annual mean zonal wind (colors), wind anomaly
531 associated with a +1 summertime Southern Annular Mode (SAM) anomaly (white contours,
532 contour interval is 0.2 m s^{-1} , negative contours dashed), and seasonal sea ice edges for the
533 summer minimum and winter maximum (defined as the 15% concentration contour, black
534 contours). 29

535 **Fig. 3.** a) Zonal-mean temperature anomaly in February per unit DJF SAM from an Argo-derived
536 dataset. Also plotted is the climatological zonal-mean ocean temperature in February with
537 a contour interval of 1°C (grey contours), the climatological zonal-mean mixed layer depth
538 in February (solid black line) and September (dashed black line) from Holte et al. (2017).
539 Blue and red boxes represent the regions in which the mixed layer and below mixed layer
540 heat content anomalies are calculated in February. b) Heat content anomalies per unit SAM
541 for cooling in the mixed layer (blue) and warming below (red). The colors are matched to
542 the boxes shown in a. Integrated anomalous surface heat flux estimates for surface heat flux
543 values of 5 and $10 \text{ W m}^{-2} \text{ K}^{-1}$ are shown by the purple and brown lines respectively. c) Sea
544 ice extent anomaly per unit DJF SAM calculated using detrended time-series. Shaded regions
545 show \pm error estimate for the regression coefficient. Using the unmodified time-series does
546 not qualitatively change the result. 30

547 **Fig. 4.** Snapshot of the temperature and sea ice fields in October (austral spring) from our idealized
548 reentrant eddy-resolving channel model using MITgcm (Marshall et al. 1997a,b). The model
549 is driven by Coordinated Ocean Research Experiments Corrected Normal Year Forcing winds
550 and fluxes. Note the presence of cold, fresh water at the surface in the region of the seasonal
551 ice zone and a pronounced temperature inversion below. 31

552 **Fig. 5.** Zonal-mean, ensemble-mean mixed layer depth from our idealized channel model, one
553 month after applying the surface forcing perturbations. The mixed layer is deeper in the
554 perturbation ensemble due to enhanced near surface mixing caused by the strengthened
555 zonal wind. Shading indicates the standard error of the mean, calculated as the standard
556 deviation of the ensemble divided by the square root of six, the number of ensemble members. . . 32

557 **Fig. 6.** Results from the eddy channel model one month after the wind perturbation is applied. a)
558 Zonal-mean temperature anomalies after one month (colors). The thin gray contours shows
559 the climatological zonal-mean temperature field from the control ensemble in February at
560 $\pm 0.5, \pm 1.5 \dots ^\circ\text{C}$, with negative contours dashed. The thick black line shows the zonal-mean
561 mixed layer depth from the perturbation ensemble. b) Zonal-mean heat budget for the region
562 of the mixed layer outlined by the blue box in a) showing that vertical diffusion dominates
563 the cooling tendency. c) Zonal-mean heat budget for the region below the zonal-mean
564 mixed layer depth outlined by the red box in a) showing that vertical diffusion dominates

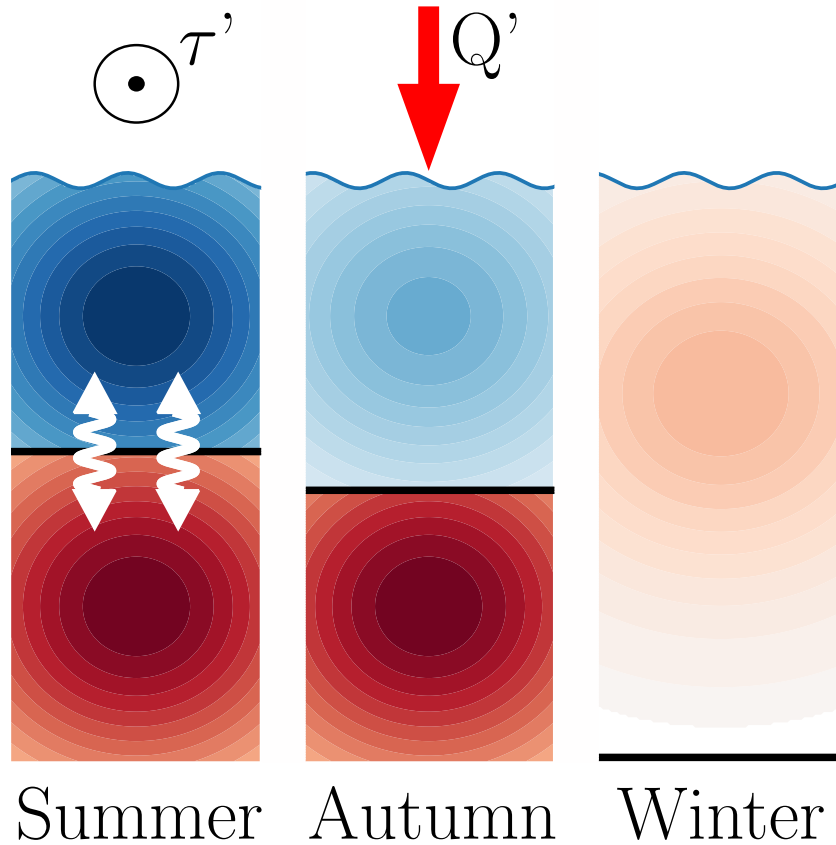
565 the warming. The vertical advection contribution is consistent with the enhanced upwelling
566 predicted by Purich et al. (2016). 33

567 **Fig. 7.** Mixed layer heat content anomaly for the channel model (blue line), for the 100 m thick
568 region below the mixed layer (orange line), the sum of these two (green line), and sea ice
569 volume anomaly (red line, right hand axis). Shading represents one standard deviation of
570 the ensemble. The x-axis is time (years) and the y-axis is either Joules or cubic meters. 34

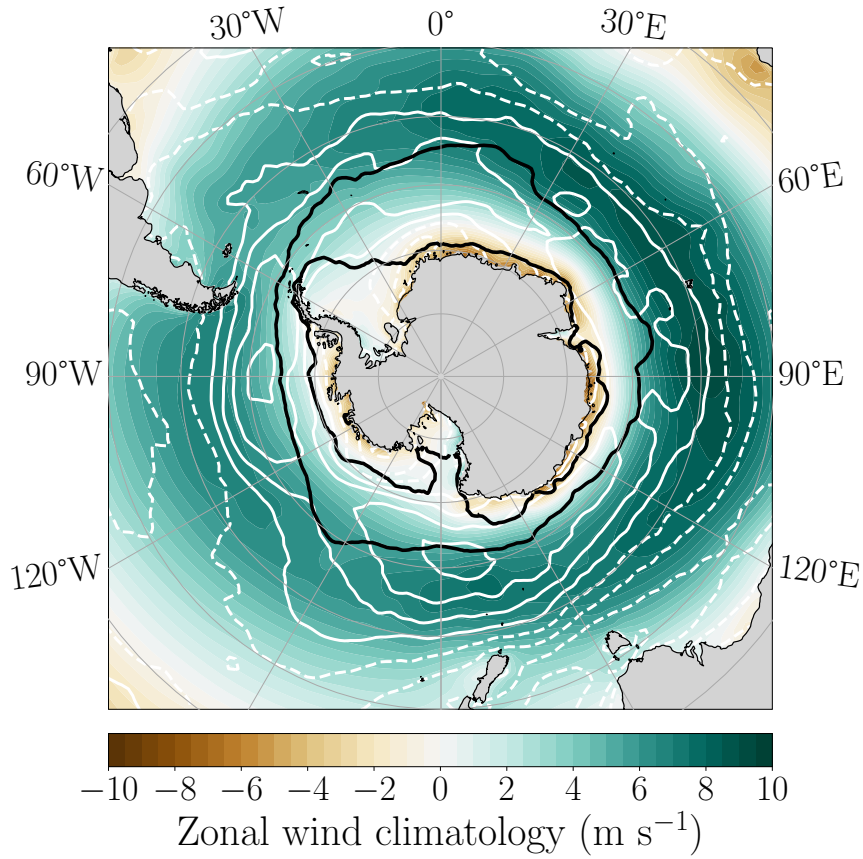
571 **Fig. 8.** Southern Ocean climatology from the preindustrial control run of the GISS global coupled
572 model. a) shows SST and sea ice concentration in February, the summertime sea ice
573 minimum. b) shows SST and sea ice concentration in September, the wintertime sea ice
574 maximum. 35

575 **Fig. 9.** a) Zonal-mean temperature anomaly in the GISS model in February of the second year
576 of the simulation. The gray contours show the climatological February temperature field
577 from the control ensemble with contours at 0, ± 1 , ± 2 , ... °C, negative and zero contours
578 are dashed. The thick black line represents the zonal-mean mixed layer depth from the
579 perturbation ensemble. b) Zonal-mean anomalous heat budget for a region in the mixed
580 layer in February of the second year, shown by the blue rectangle in a). Advection makes
581 the largest contribution to the anomalous cooling. Mixing contributes only about one fifth
582 as much cooling as advection. c) Zonal-mean anomalous heat budget for a region below the
583 zonal-mean mixed layer depth in February of the second year. The region is shown by the
584 red rectangle in a). Mixing is largely responsible for the anomalous warming. (Note that the
585 vertical scale in c is an order of magnitude smaller than b.) 36

586 **Fig. 10.** Correlations between SAM and other model fields from the GISS control simulation. a)
587 Zonal-mean February temperature anomaly per unit DJF SAM. Gray contours show cli-
588 matological zonal-mean temperature field in February with contours at 0, ± 1 , ± 2 , ... °C,
589 negative and zero contours are dashed. Black line represents climatological zonal-mean
590 mixed layer depth in February from the control ensemble. b) Ocean heat content anomalies
591 calculated using the zonal-mean temperature perturbations and regions shown in a). Blue
592 line represents mixed layer box, red line represents box below mixed layer. Consistent with
593 the diagnostics in figure 9, the sum of the two heat content anomalies is negative (gray line),
594 showing that vertical redistribution is not the only process cooling the mixed layer. c) The
595 sea ice area (blue) and volume (orange) anomalies per unit SAM. Both show a transient
596 increase, but only sea ice volume shows a reduction in the following winter. After applying
597 a Bonferroni correction none of the regression coefficients are statistically discernible from
598 zero. 37

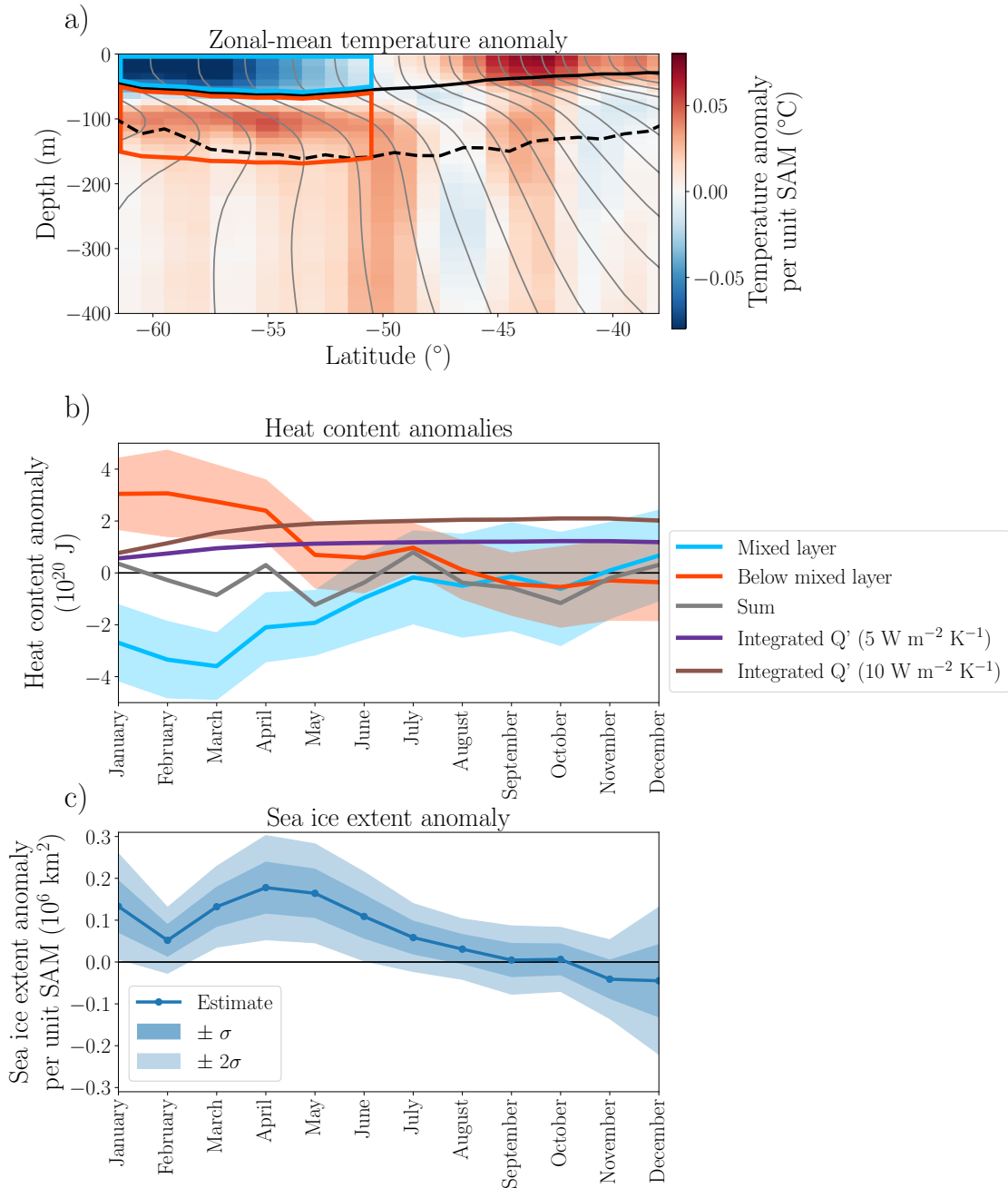


599 FIG. 1. Schematic of vertical mixing/heat sequestration mechanism. In summer, anomalous westerly winds
 600 (τ' above left hand column) enhance vertical mixing at the base of the mixed layer (white squiggly arrows
 601 and horizontal black line, respectively) moving heat downwards and causing a vertical dipole of anomalous
 602 temperatures (colors). The anomalously cold SST causes anomalous heat fluxes into the ocean during the
 603 autumn (Q' and red arrow above central column), which reduces the cold SST anomaly. As autumn progresses,
 604 the mixed layer continues to deepen, entraining the anomalously warm fluid sequestered below the zonal-mean
 605 mixed layer depth. Due to the anomalous surface heat fluxes, which increases the total heat content of the upper
 606 ocean, the mixed layer is now anomalously warm. This can be expected to lead to a reduction in wintertime sea
 607 ice.

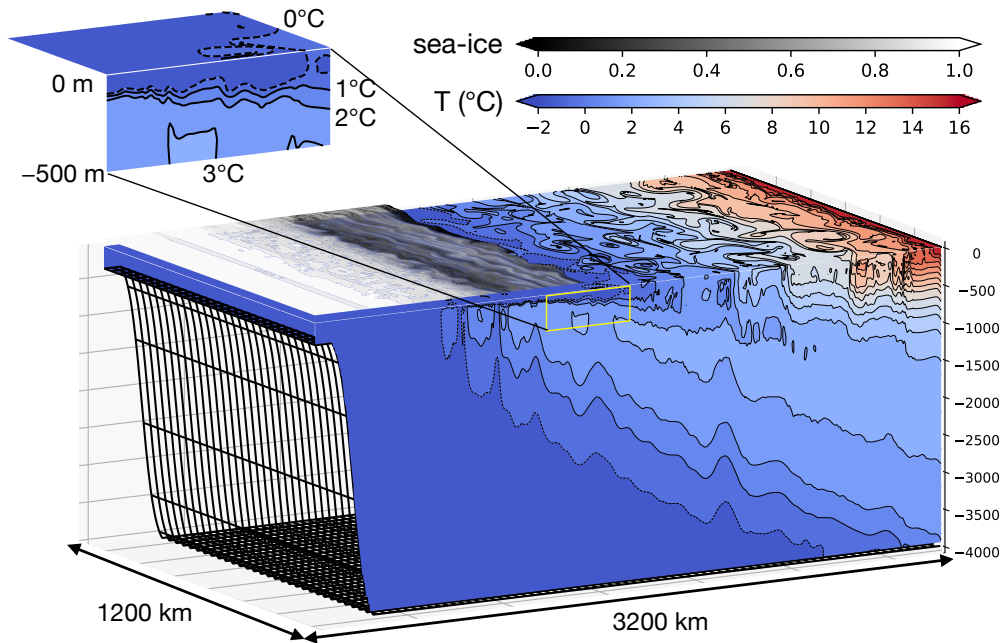


608 FIG. 2. Climatology of the Southern Ocean. Annual mean zonal wind (colors), wind anomaly associated
 609 with a +1 summertime Southern Annular Mode (SAM) anomaly (white contours, contour interval is 0.2 m s^{-1} ,
 610 negative contours dashed), and seasonal sea ice edges for the summer minimum and winter maximum (defined
 611 as the 15% concentration contour, black contours).

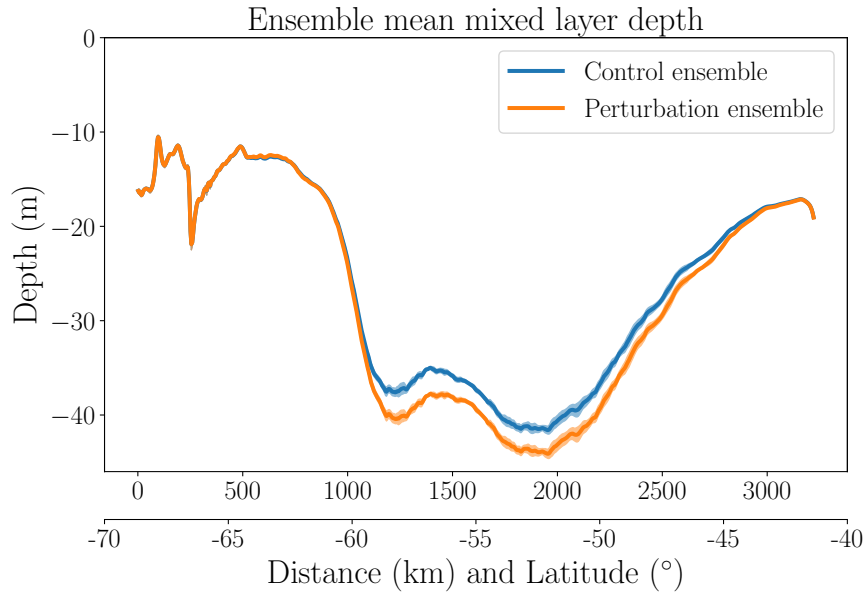
Observations



612 FIG. 3. a) Zonal-mean temperature anomaly in February per unit DJF SAM from an Argo-derived dataset.
 613 Also plotted is the climatological zonal-mean ocean temperature in February with a contour interval of 1°C
 614 (grey contours), the climatological zonal-mean mixed layer depth in February (solid black line) and September
 615 (dashed black line) from Holte et al. (2017). Blue and red boxes represent the regions in which the mixed layer
 616 and below mixed layer heat content anomalies are calculated in February. b) Heat content anomalies per unit
 617 SAM for cooling in the mixed layer (blue) and warming below (red). The colors are matched to the boxes shown
 618 in a. Integrated anomalous surface heat flux estimates for surface heat flux values of 5 and $10 \text{ W m}^{-2} \text{K}^{-1}$ are
 619 shown by the purple and brown lines respectively. c) Sea ice extent anomaly per unit DJF SAM calculated using

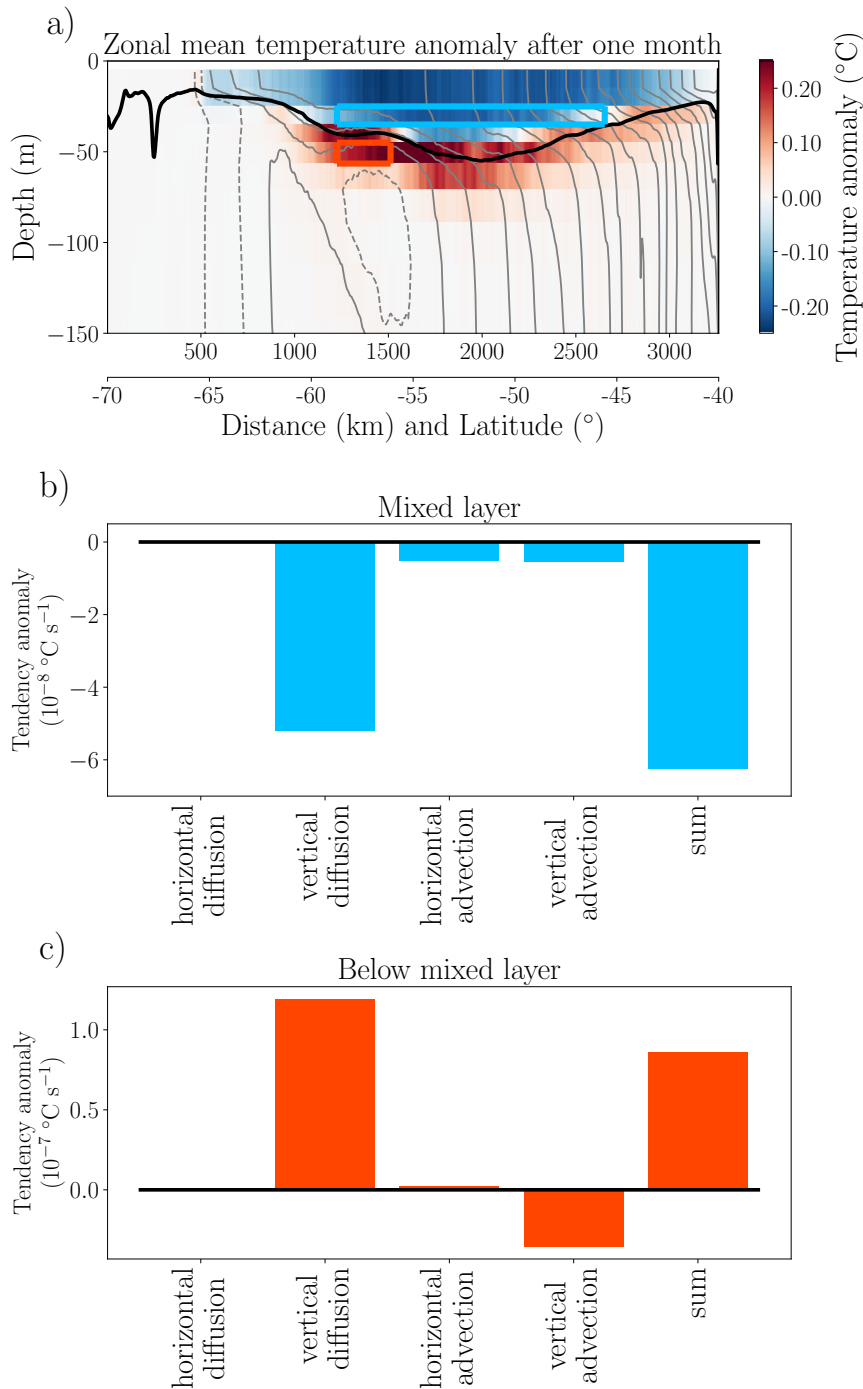


622 FIG. 4. Snapshot of the temperature and sea ice fields in October (austral spring) from our idealized reentrant
 623 eddy-resolving channel model using MITgcm (Marshall et al. 1997a,b). The model is driven by Coordinated
 624 Ocean Research Experiments Corrected Normal Year Forcing winds and fluxes. Note the presence of cold, fresh
 625 water at the surface in the region of the seasonal ice zone and a pronounced temperature inversion below.



626 FIG. 5. Zonal-mean, ensemble-mean mixed layer depth from our idealized channel model, one month after
 627 applying the surface forcing perturbations. The mixed layer is deeper in the perturbation ensemble due to
 628 enhanced near surface mixing caused by the strengthened zonal wind. Shading indicates the standard error of
 629 the mean, calculated as the standard deviation of the ensemble divided by the square root of six, the number of
 630 ensemble members.

Channel Model



631 FIG. 6. Results from the eddy channel model one month after the wind perturbation is applied. a)

632 Zonal-mean temperature anomalies after one month (colors). The thin gray contours shows the climatological

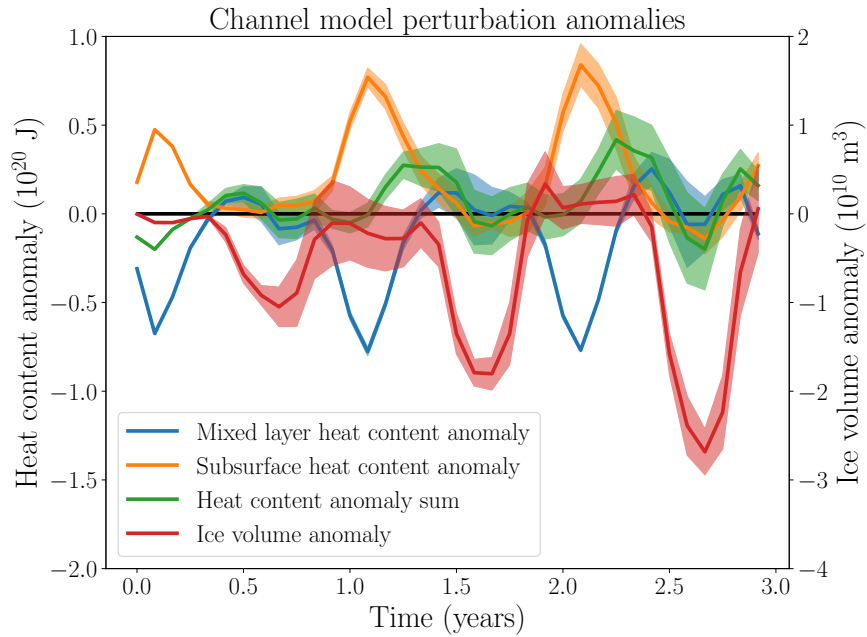
633 zonal-mean temperature field from the control ensemble in February at $\pm 0.5, \pm 1.5 \dots$ $^{\circ}\text{C}$, with negative contours

634 dashed. The thick black line shows the zonal-mean mixed layer depth from the perturbation ensemble. b)

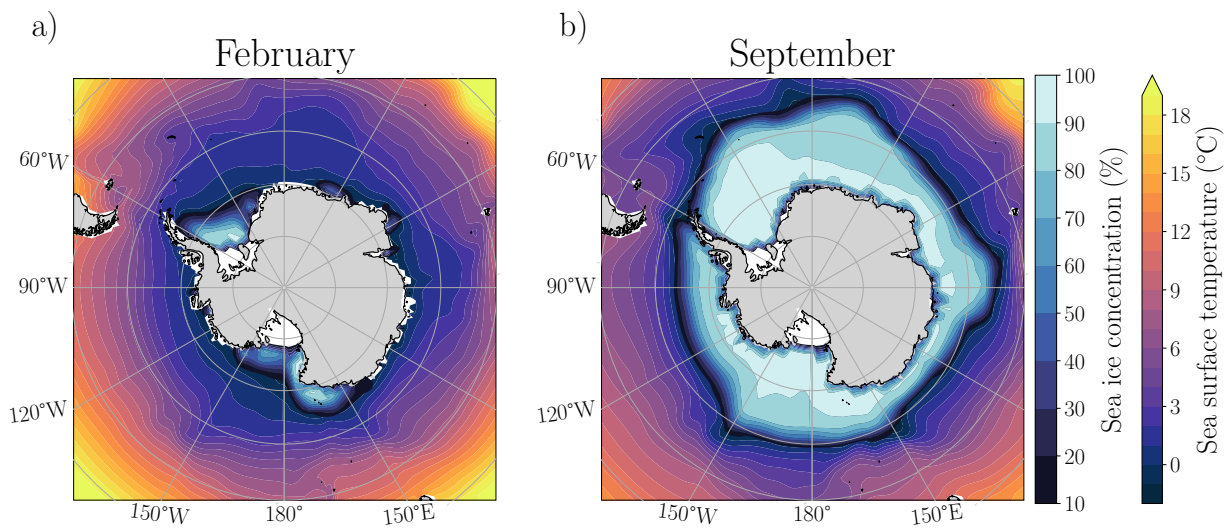
635 Zonal-mean heat budget for the region of the mixed layer outlined by the blue box in a) showing that vertical

636 diffusion dominates the cooling tendency. c) Zonal-mean heat budget for the region below the zonal-mean mixed

637 layer depth outlined by the red box in a) showing that vertical diffusion dominates the warming. The vertical

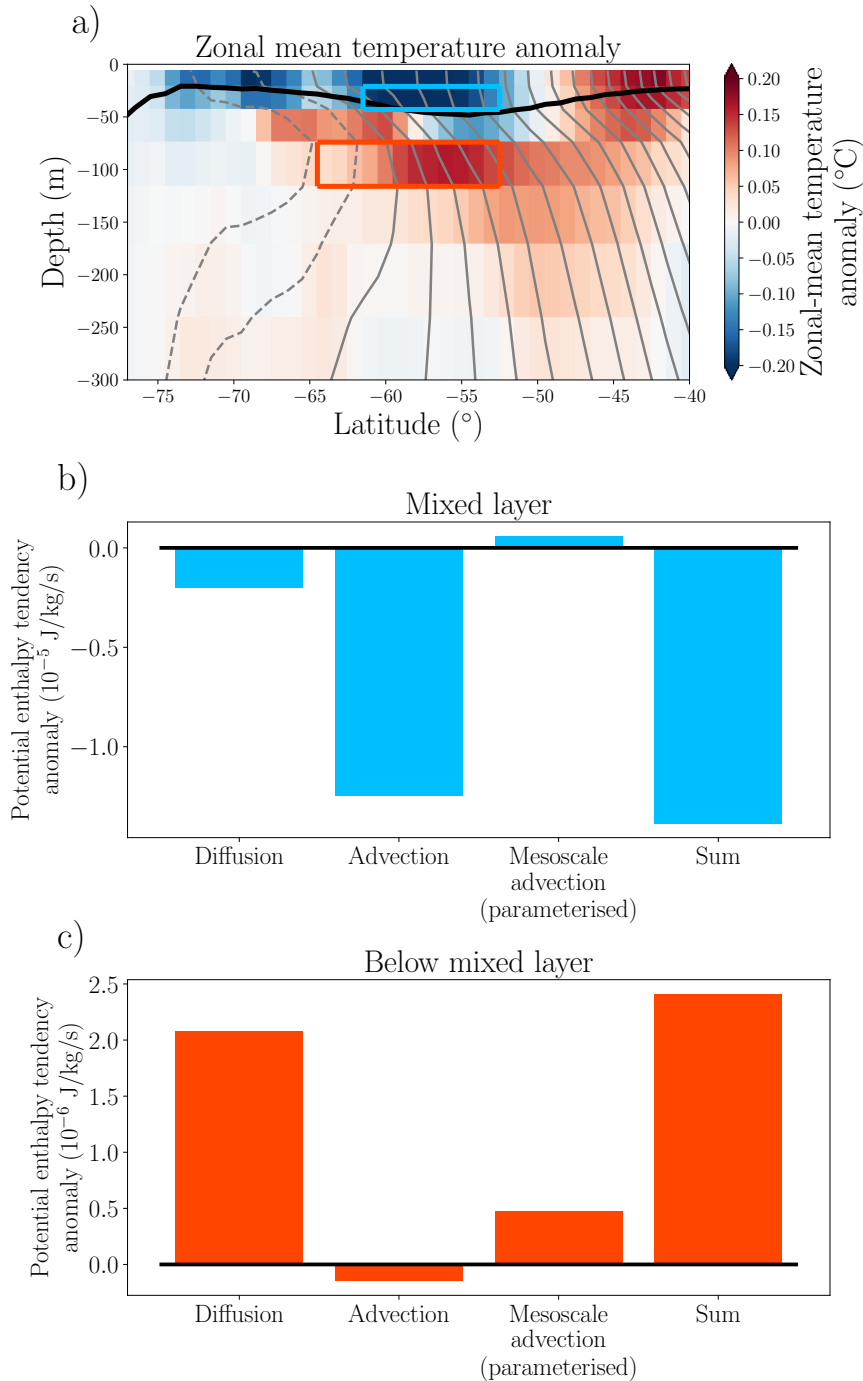


639 FIG. 7. Mixed layer heat content anomaly for the channel model (blue line), for the 100 m thick region below
 640 the mixed layer (orange line), the sum of these two (green line), and sea ice volume anomaly (red line, right hand
 641 axis). Shading represents one standard deviation of the ensemble. The x-axis is time (years) and the y-axis is
 642 either Joules or cubic meters.

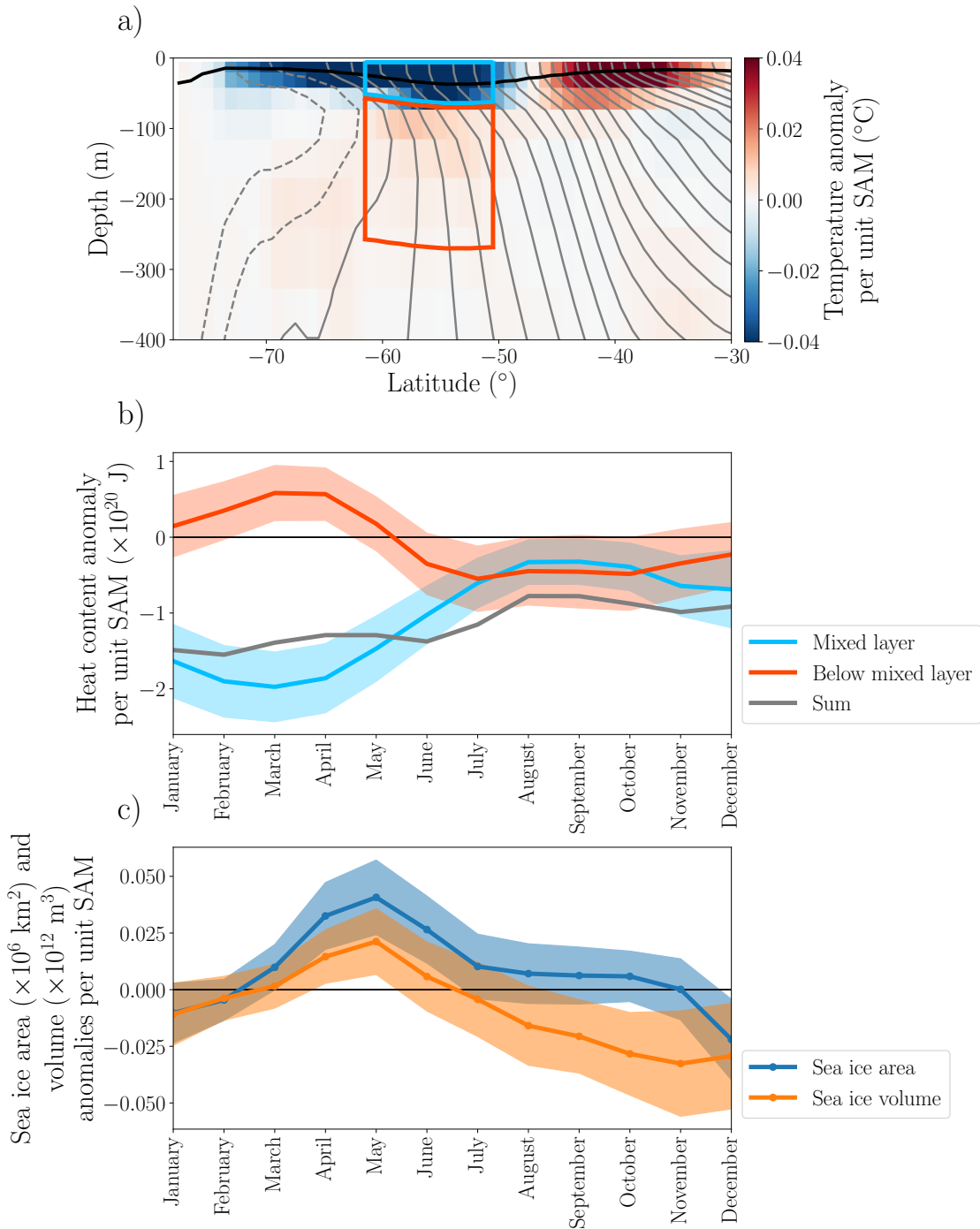


643 FIG. 8. Southern Ocean climatology from the preindustrial control run of the GISS global coupled model. a)
 644 shows SST and sea ice concentration in February, the summertime sea ice minimum. b) shows SST and sea ice
 645 concentration in September, the wintertime sea ice maximum.

GISS Model



646 FIG. 9. a) Zonal-mean temperature anomaly in the GISS model in February of the second year of the simulation.
 647 The gray contours show the climatological February temperature field from the control ensemble with contours
 648 at $0, \pm 1, \pm 2, \dots$ $^{\circ}\text{C}$, negative and zero contours are dashed. The thick black line represents the zonal-mean mixed
 649 layer depth from the perturbation ensemble. b) Zonal-mean anomalous heat budget for a region in the mixed
 650 layer in February of the second year, shown by the blue rectangle in a). Advection makes the largest contribution
 651 to the anomalous cooling. Mixing contributes only about one fifth as much cooling as advection.
 652 c) Zonal-mean anomalous heat budget for a region below the zonal-mean mixed layer depth in February of the second year. The



655 FIG. 10. Correlations between SAM and other model fields from the GISS control simulation. a) Zonal-mean
 656 February temperature anomaly per unit DJF SAM. Gray contours show climatological zonal-mean temperature
 657 field in February with contours at 0, ± 1 , ± 2 , ... $^{\circ}\text{C}$, negative and zero contours are dashed. Black line
 658 represents climatological zonal-mean mixed layer depth in February from the control ensemble. b) Ocean heat
 659 content anomalies calculated using the zonal-mean temperature perturbations and regions shown in a). Blue line
 660 represents mixed layer box, red line represents box below mixed layer. Consistent with the diagnostics in figure
 661 9, the sum of the two heat content anomalies is negative (gray line), showing that vertical redistribution is not
 662 the only process cooling the mixed layer. c) The sea ice area (blue) and volume (orange) anomalies per unit